

# Search for Precessing Binary Black Holes in Advanced LIGO’s Third Observing Run using Harmonic Decomposition

Rahul Dhurkunde and Ian Harry

*Institute of Cosmology and Gravitation, University of Portsmouth, Portsmouth, PO1 3FX, U.K.*

(Dated: January 9, 2026)

Binary black holes (BBHs) exhibiting spin-induced orbital precession offer unique insight into compact-binary formation channels, cosmology, and tests of general relativity. We conduct a dedicated search for precessing BBHs in Advanced LIGO’s third observing run (O3) using the harmonic decomposition method of precessing waveforms. We introduce a novel scheme to reduce the number of filters in a harmonic search. With our new approach, our template bank requires  $5\times$  fewer filters compared to another proposed precessing search in the same region. We do not find any new significant events. Our new search method achieves up to  $\sim 28\%$  improvement in sensitivity and up to  $5\times$  lower computational costs compared to existing precessing search pipelines. Our method enables scalable, sensitive searches for precessing BBHs in future gravitational-wave observing runs.

## I. INTRODUCTION

The discovery of gravitational waves (GWs) has improved our understanding of compact binary systems – binaries involving black holes and/or neutron stars [1]. When the spins of these black holes are misaligned with the orbital angular momentum, the orbital plane undergoes precession [2]. This spin-orbit coupling effect leads to characteristic amplitude and phase modulations in the emitted gravitational waves, which are strongest for binaries with large in-plane spin components, asymmetric masses, or edge-on orientations [3–6]. Such configurations are expected in a variety of astrophysical scenarios.

Precessing binaries can form through multiple evolutionary channels [7–9]. In isolated binary evolution, supernova kicks imparted during the formation of compact objects can misalign the spins from the orbital angular momentum [10, 11]. Alternatively, in dynamically formed systems—such as those originating in globular clusters, nuclear star clusters, or hierarchical triples—the orientations of spins are expected to be nearly isotropic [7, 12, 13].

The detection and precise characterization of precessing binaries have significant implications for several domains. From an astrophysical perspective, clear measurement of precession can offer insights into the formation environments of compact binaries [1, 14]. Observational evidence of spin-induced precession is a more likely signature of a dynamical formation over an isolated channel, and may help estimate the relative rates of the various formation channels. For cosmology using GWs, precession can help break the inclination-distance degeneracy [15], resulting in better estimates of the redshifts for these sources, which in turn can give better estimates of the Hubble constant via Dark vs. Bright siren cosmological methods [16]. Furthermore, precessing binaries can provide cleaner tests of general relativity in the strong-field regime by breaking mode degeneracies and enhancing the spectral sensitivity of ringdown tests to deviations from the Kerr

metric [17]. Precessing signals can also provide tests of the large-scale symmetries of the Universe [18].

As of the latest release, the Gravitational-Wave Transient Catalog 4 (GWTC-4) [19] contains nearly two hundred well-characterized binary mergers detected by the Advanced LIGO [20] and Advanced Virgo [21] detectors. The majority of these events are consistent with aligned-spin systems [1]. A population-level analysis comparing observations from the catalogs GWTC-3 [22] to GWTC-4 reveals an increasing preference for systems with  $\chi_P > 0$  (see Figure 8 of [1]), where  $\chi_P$  is the effective precession parameter introduced in [23]. A few events show potential evidence for orbital precession, with GW200129.065458 to be the strongest so far: the event has been measured to have a precessing frequency (the rate at which the orbital plane rotates) of at least 1 Hz when the signal enters the LIGO sensitive band [24]. The scarcity of confidently identified precessing signals may point to astrophysical reality [25] or reflect the limitations of current detection pipelines, which are predominantly optimized for aligned-spin binaries.

Modeled gravitational-wave searches typically use a bank of filters (templates) to perform matched filtering of the interferometric data [26–30]. Standard searches use template banks restricted to aligned-spin configurations due to computational efficiency and a simpler matched-filter statistic. For an aligned-spin search, the effects of varying the unknown extrinsic parameters of a binary – such as sky-location and inclination angle of the binary plane can be incorporated as a fiducial amplitude and overall phase to the gravitational-wave signal. In such cases, the matched filter can be conveniently performed with templates that depend only on four parameters – component masses and spins restricted parallel to the orbital angular momentum. The same does not hold true for precessing systems, as the signal seen by a detector is phase and/or amplitude modulated by varying inclination angle, sky-location or due to time-varying component spins. Aligned-spin template banks have poor ability to capture generically precessing signals due to omission of precessional effects [3, 4, 31–33]. Specifically for highly

precessing BBH systems, aligned-spin banks can lose up to 25% of signal-to-noise ratio (SNR) [33]. Although unmodeled pipelines and semi-analytical strategies exist, they struggle to match the sensitivity of matched-filtering techniques for low-mass systems [34–36].

Several methods have been proposed to detect precessing compact binary mergers in the past, but most of them have struggled with balancing sensitivity with computational cost. Parameter-modulated templates improved matches modestly but increased noise and [37], while later approaches allowing free maximization over waveform coefficients led to unphysical solutions and higher false-alarm rates [38]. Fully physical template banks covering all parameters were also attempted but proved computationally infeasible, requiring tens of millions of templates [4]. Despite the challenges, there have been two precessing searches performed on the O3 data from Advanced LIGO detectors: one for binary black holes (BBHs) [39], and for neutron star-black hole binaries [40]. No new candidates were found w.r.t the existing aligned-spin searches [19] in any of the precessing searches.

The decomposition of any precessing signal into multiple harmonics offers a promising path to perform precessing searches [41]. Related formalisms for single-spin binaries were introduced earlier in [42, 43]. As recently demonstrated in [40], the harmonic precessing search for NSBH systems requires  $3\times$  fewer templates than brute-force approaches, and is up to 100% more sensitive than an equivalent aligned-spin search. In this work, we use an improved implementation of the same harmonic decomposition technique to perform a full-scale search for highly precessing BBH systems. We introduce a new technique that substantially reduces the number of filters required for the harmonic search. With this method, we achieve a fivefold reduction in filters compared to the previous search for highly precessing BBHs [39], while simultaneously achieving significantly improved fitting factors across the template bank.

In this work we search using publicly available data from the Advanced LIGO detectors during their third observing run [44]. We choose the same parameter space as the most recent search for precessing BBHs [39] Our search region covers as shown in Figure 1 : detector frame component masses  $m_1^{\text{det}} \in [15, 70]M_\odot$ ,  $m_2^{\text{det}} \in [3, 10]M_\odot$  with a cutoff on mass-ratio  $q = m_1^{\text{det}}/m_2^{\text{det}} \in [5, 12]$ . We did not find any new significant events and recover 29 events that were previously reported in the latest GWTC-4 catalog [1]. Our precessing search combined with an equivalent search is up to 28% more sensitive than an aligned-spin only search and requires  $5\times$  fewer filters than a previous precessing search in the same region.

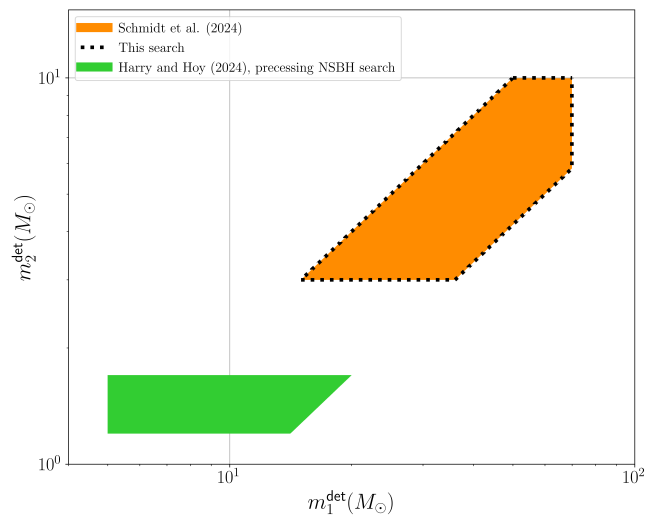


FIG. 1. Search region of the previous precessing searches in the O3 data of the Advanced LIGO detectors for compact binary mergers to-date. Shown is the search region as the two dimensional space of detector frame component masses ( $m_1^{\text{det}}, m_2^{\text{det}}$ ). The green area denotes the parameter space explored in the recent NSBH precessing search that employed the same harmonic decomposition technique [41, 45]. The orange area corresponds to the region used in the highly precessing BBH search of [39]. We have chosen the exact same parameter region as the previous precessing BBH search (marked as black dotted lines).

## II. SEARCH FOR ORBITAL PRECESSION USING HARMONICS

The harmonic-decomposition formalism for detecting single-spin precessing systems was introduced in [42, 43] and for fully-precessing systems in [41], the latter was implemented as a complete end-to-end search framework in [45], and subsequently applied to advanced LIGO data to search for precessing NSBH binaries in [40]. In this work, we primarily build on the implementation of [45], supplemented with new enhancements that further improve the efficiency of the harmonic search. Sections II A–II E review the methodology for conducting a harmonic-based search, and Section II F details the improvements introduced in this study.

### A. Harmonic decomposition of precessing waveforms

Consider a precessing binary system in a quasi-circular orbit with an orbital angular momentum  $\mathbf{L}$  and spin angular momentum vectors for each component  $\mathbf{S}_1, \mathbf{S}_2$ . The total angular momentum is given by  $\mathbf{J} = \mathbf{L} + \mathbf{S}_1 + \mathbf{S}_2$ . The gravitational waveform emitted by the binary as seen

by the detector is expressed approximately as [46]

$$h(t) = - \left( \frac{d_0}{d_L} \right) A_0(t) \times \quad (1)$$

$$\text{Re} \left[ e^{2i\Phi_s(t)} \left( F_+(C_+ - iS_+) + F_\times(C_\times - iS_\times) \right) \right],$$

where  $A_0(t)$  is the time-varying amplitude which depends upon the component masses and spins of the binary, and we have separated the luminosity distance  $d_L$  dependence as the waveform defined at a fiducial distance  $d_0$ .  $F_+$  and  $F_\times$  are the detector response (relative to  $\mathbf{J}$ -frame) functions, and  $C_{+,\times}, S_{+,\times}$  are the time-varying response to the gravitational wave.

The phase  $\Phi_s(t)$  is defined in the frame aligned with  $\mathbf{J}$ , and its evolution is related to the orbital phase  $\phi_{orb}$  as

$$\Phi_s(t) = \phi_{orb}(t) - \epsilon(t), \quad (2)$$

where the binary precesses with rate  $\dot{\epsilon}$  given as

$$\dot{\epsilon}(t) = \dot{\alpha} \cos \beta(t), \quad (3)$$

and  $\beta$  is the opening angle between  $\mathbf{J}$  and  $\mathbf{L}$  and  $\dot{\alpha}(t)$  is the precession frequency. Using the parameter

$$b = \tan(\beta/2), \quad (4)$$

one can write the responses  $C_{+,\times}, S_{+,\times}$  in terms of  $(\theta_{\text{JN}}, \beta, \alpha)$  where  $\theta_{\text{JN}}$  is the angle between  $\mathbf{J}$  and the line-of-sight to the observer. Following [41], rewriting the equation (2) as

$$h(t) = \text{Re} \left[ \left( \frac{A_0(t) e^{2i(\Phi_s + \alpha)}}{(1 + b^2)^2} \right) \quad (5)$$

$$\sum_{k=0}^4 (b e^{-i\alpha})^k (F_+ \mathcal{A}_k^+ - i F_\times \mathcal{A}_k^\times) \right],$$

where the amplitudes  $\mathcal{A}_k^{+,\times}$  depend on  $\theta_{\text{JN}}$  and  $d_L$  and are explicitly given in [41]. Factorizing out the dependence of orbital  $\phi_{orb}$  and precession phase  $\Phi_s$ , the binary's phase evolution is written as [41]

$$\Phi(t) = \Phi_s(t) - \Phi_0 + \alpha(t) - \alpha_0. \quad (6)$$

Following [45], we can then write the observed signal as

$$h(t) = \sum_{k=0}^4 A_k h_k(t) e^{i\phi_k(t)}, \quad (7)$$

where

$$h_k(t) = \frac{A_0(t) b^k(t)}{(1 + b^2(t))^2} e^{i[2\Phi(t) - k(\alpha(t) - \alpha_0)]}, \quad (8)$$

$$A_k = ((F_+ \mathcal{A}_k^+)^2 + (F_\times \mathcal{A}_k^\times)^2)^{1/2}, \quad (9)$$

and

$$\phi_k = 2\Phi_0 + (2 - k)\alpha_0 - \tan^{-1} \left( \frac{F_\times \mathcal{A}_k^\times}{F_+ \mathcal{A}_k^+} \right) \quad (10)$$

From the equations (7), (9) and (10), we see that any variation in the extrinsic parameters changes only the overall amplitudes and phases of each harmonic which do not vary over time. We note that, for a generic precessing binary,  $\beta$  can range between  $[0, \pi)$ , and therefore,  $b \in [0, \infty)$ . For aligned / anti-aligned systems  $b$  is either close to zero or is a large positive number, for maximally precessing configuration  $b \sim 1$ . From equation (8), we see that the harmonic amplitudes roughly scale proportionally to  $b^k$ . Similar to the time-domain harmonics, the Fourier domain ones can be obtained by using the stationary phase approximation, and the precessing waveform can be written as

$$\tilde{h}(f) = \text{Re} \sum_{k=0}^4 A_k \tilde{h}_k(f) e^{i\phi_k}, \quad (11)$$

where  $\tilde{h}(f)$  is the Fourier transform of  $h(t)$ .

## B. Filtering with orthonormalized harmonics

Modeled searches employ the matched filtering technique to estimate the likelihood of data  $s$  containing a modeled gravitational signal  $h$  [47, 48]. Matched filter is an optimal detection statistic under the assumption that data contains *Gaussian* and *stationary* noise. The matched filter is performed in the Fourier domain, by correlating the Fourier-transformed data  $\tilde{s}(f)$  and a template  $\tilde{h}(f)$  of the anticipated signal, weighted by the noise power spectral density (PSD)  $S_n(f)$ . The complex matched filter statistic is given by

$$\langle h|s \rangle = 4 \int \frac{\tilde{h}^*(f) \tilde{s}(f)}{S_n(f)} df, \quad (12)$$

$$\langle h|s \rangle = \text{Re}[\langle h|s \rangle]. \quad (13)$$

The signal-to-noise ratio (SNR) is defined as

$$\rho^2 = \frac{\langle h|s \rangle^2}{\langle h|h \rangle}. \quad (14)$$

A binary system in a quasi-circular orbit is characterized by 15 parameters: component masses  $(m_1, m_2)$ , component spin vectors  $\vec{s}_1, \vec{s}_2$ , inclination angle  $i$ , sky-location angles  $(\theta, \delta)$ , polarization  $\psi$ , luminosity distance to the source  $d_L$ , the orbital phase  $\phi_c$  and time  $t_c$  at binary coalescence. A priori, the signal parameters are unknown, so the matched filter statistic is maximized over a wide range of possibilities to maximize the likelihood of finding a real gravitational-wave signal. Therefore, a discrete set of filters (templates) are used to search over a given region of the parameter space. For aligned-spin signals, varying extrinsic parameters such as inclination and sky-location change only the amplitude or an overall phase to the signal. In such cases, all the extrinsic parameters except  $(m_1, m_2, s_{1z}, s_{2z})$  are

analytically maximized by taking the absolute of the complex matched filter output

$$\max(\rho^2) = |\langle h|s \rangle|^2. \quad (15)$$

The remaining parameters are included in the template bank.

To perform matched filtering for precessing signals, we use the Fourier transformed harmonic components described in (11). If the five harmonics were independent, each could be matched-filtered separately while maximizing over the respective fiducial phase  $\phi_k$  and amplitude  $A_k$  parameters. However, their non-orthogonality introduces covariance among the matched-filter outputs, complicating the maximization of the SNR. To simplify this, we first orthonormalize the harmonics using Gram-Schmidt orthogonalization, according to the following equations:

$$h_k^\perp = h_k - \sum_{l=0}^{k-1} (h_l | h_k) h_l, \quad (16)$$

$$\hat{h}_k = \frac{h_k^\perp}{(h_k^\perp | h_k^\perp)}. \quad (17)$$

An example of orthonormalized harmonics is shown in the Figure 2. We use these new orthonormalized harmonics, and filter each of them separately for the corresponding templates. The SNR for each harmonic is obtained by independently maximizing over the unknown amplitudes  $A_k$  and phases  $\phi_k$  and then combining in quadrature to get the total SNR for the given template

$$\rho_h^2 = \sum_{k=0}^4 \max_{A_k, \phi_k} [\rho_k]^2, \quad (18)$$

where  $\rho_k = (h_k^\perp | s)$  is the matched-filter output by filtering using the  $k^{\text{th}}$  orthogonalized harmonic. In the next section we describe the procedure for constructing a harmonic template bank.

### C. Constructing the template bank

A bank of templates is used to search over the intrinsic parameters of the expected signal. Several sampling strategies exist in the literature to ensure adequate coverage of the parameter space [49, 50]; only a small fraction of injections within the bank's domain should have a best match below the prescribed minimum match. The best match achieved between a signal and the templates in the bank is known as the fitting factor, which corresponds to the fraction of a signal  $g$ 's SNR that is recovered by a given template  $h$ :

$$\text{FF}(g) = \max_{i \in \text{bank}} [m(h_i, g)]. \quad (19)$$

Parameter	Range
$m_1$	$[15, 70]M_\odot$
$m_2$	$[3, 10]M_\odot$
$q$	$[5, 12]$
$ s_1 $	$[0.5, 0.9]$
$ s_2 $	$[0.0, 0.99]$
$\phi_c$	$[0, 2\pi]$
$i$	$[0, \pi]$
$(\alpha, \delta)$	$([0, 2\pi], [0, \pi])$
$\psi$	$[0, 2\pi]$

Precessing bank

Parameter	Range
$m_1$	$[15, 70]M_\odot$
$m_2$	$[3, 10]M_\odot$
$q$	$[5, 12]$
$ s_{1z} $	$[0.0, 0.99]$
$ s_{2z} $	$[0.0, 0.99]$

Aligned-spin bank

TABLE I. Description of the template banks used in this work – our precessing bank and an equivalent aligned-spin bank. We show the parameters that are used to create the discrete set of templates and their respective ranges. Both template banks are created with a stochastic sampling method with a minimum match requirement of 0.97. Our precessing bank contains 13 parameters (spans 8 parameters – component masses and generic spins) and has 211,730 templates. The equivalent aligned-spin bank has only 4 parameters with spins restricted to only in the  $z$  direction and contains 33099 templates.

The stochastic sampling is done iteratively by checking the match of a proposed template  $h_{\text{prop}}$  against the harmonic decomposition of the existing templates  $h_i$  in the bank. Since the amplitudes and phases ( $A_k, \phi_k$ ) depend on the extrinsic parameters, and so does the match for the proposed template. Therefore, we fix the sky-location and orientation when computing the match for  $h_{\text{prop}}$  using all five components. If the fitting factor is still less than the mismatch, then  $h_{\text{prop}}$  is added to the bank.

In this search we consider only the dominant mode of gravitational emission. We use the IMRPhenomXP approximant to model precessing signals [51, 52]. While computing the matches, we generate the templates with a lower frequency cutoff of 15Hz and use the O3 optimistic PSD [53]. We use the sbank library to generate our bank with a minimum match = 0.97. Our template bank spans 8 dimensions: detector frame component masses ( $m_1^{\text{det}}, m_2^{\text{det}}$ ) and generic component spins ( $s_{1x}, s_{1y}, s_{1z}, s_{2x}, s_{2y}, s_{2z}$ ). In our bank, we also store the fixed sky-location  $(\theta, \delta)$ , inclination  $i$ , polarization  $\psi$  and coalescence phase  $\phi_c$  used while computing the matches for generating the bank. The parameter ranges used for our bank are described in Table I.

Our precessing template bank contains 211,730 templates—an order of magnitude smaller than the bank used in the previous precessing BBH search [39], which comprised approximately  $2.3 \times 10^6$  templates. The bank in [39] was constructed with a mismatch of 0.9; applying

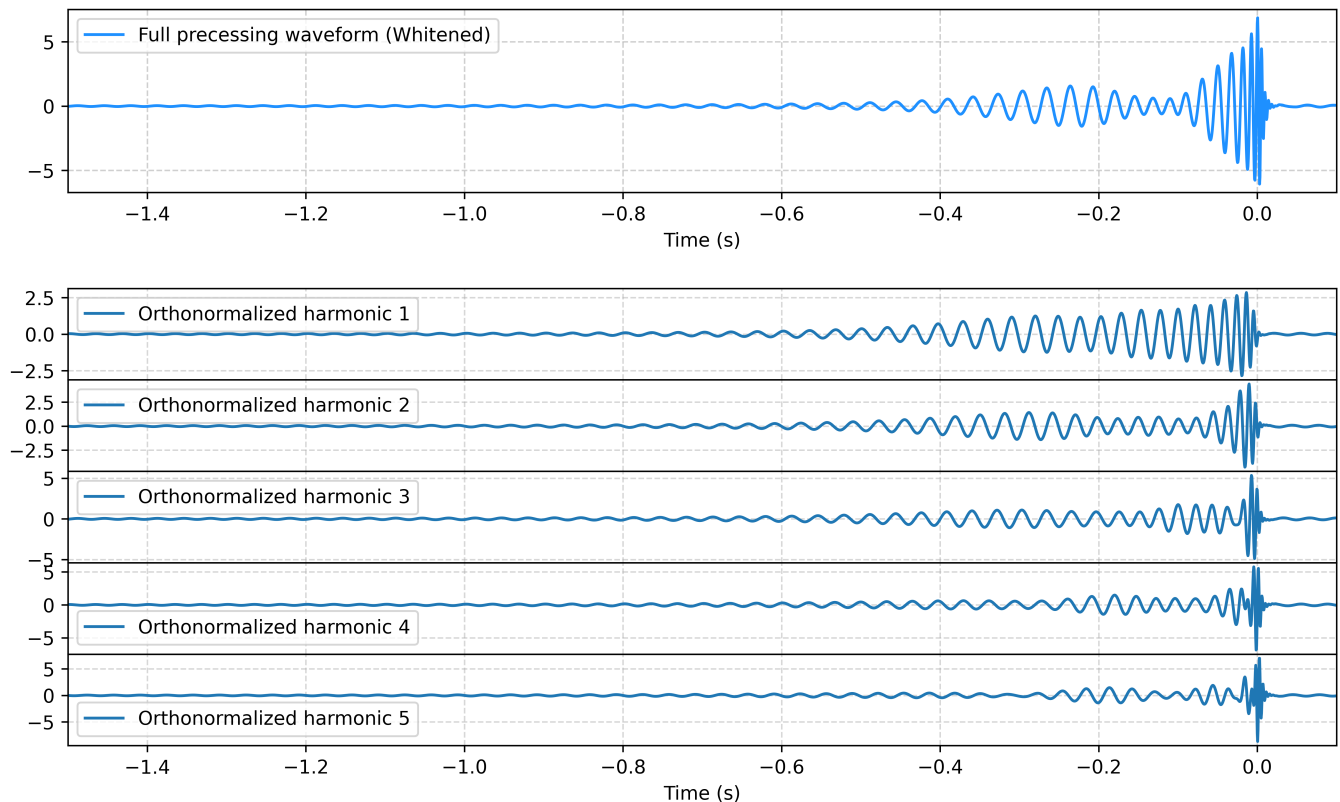


FIG. 2. Whitened precessing waveform and the orthonormalized harmonic decomposition of the same waveform in the time-domain. On the top is the full whitened precessing waveform for a binary with  $(m_1^{\text{det}}, m_2^{\text{det}}) = (57.5, 5.7)M_\odot$ , inclination  $\sim 74^\circ$  and  $b = 0.93$  generated using IMRPhenomXP. The second to sixth rows correspond to the orthonormalized harmonics, with the first being the dominant harmonic, followed by second then third and so on.

the same method with a mismatch of 0.97 would produce more than 30 million templates.

For comparison, we also construct an aligned-spin template bank by sampling over the same parameter region but restricting the spins to be aligned with the orbital angular momentum, with spin magnitudes constrained to  $(|s_{1z}|, |s_{2z}|) \in [0.0, 0.99]$ . The templates are generated using IMRPhenomXAS [51], employing the same lower-frequency cutoff and PSD for all match calculations. This aligned-spin bank spans the four parameters  $(m_1^{\text{det}}, m_2^{\text{det}}, s_{1z}, s_{2z})$  and consists of 33,099 templates.

#### D. Reducing the number of filters

Using all five harmonics for each template is computationally expensive, and is not necessary as not every template requires all five harmonics: templates which are aligned-spin like can be accurately represented by the dominant harmonic only, whereas precessing templates (significant in-plane spin components) would require more than just the dominant harmonic. Therefore, we pre-compute the number of harmonics required by each template. We estimate this by

computing an *effective match*  $m_{\text{eff}}$  of each template  $h_i$ , which is an averaged match over a sufficient  $n$  random sky-location and orientation (denoted by  $\Omega$ ) for the same system i.e. keeping the other parameters fixed. The effective match is computed as

$$m_{\text{eff}}(h_i) = \left[ \frac{m(h_i, h_i(\Omega))^3 \rho_{\text{opt}}^3}{\sum_{i=0}^n \rho_{\text{opt}}^3(h_i)} \right]^{1/3}, \quad (20)$$

where  $\rho_{\text{opt}}$  is the optimal SNR of the given template with itself or in other words the complete set of the orthonormalized harmonics

$$\rho_{\text{opt}} = \left[ \sum_{k=0}^4 |(\hat{h}_k^\perp | h)|^2 \right]^{1/2}. \quad (21)$$

We calculate the effective match by successively increasing the number of harmonics until it reaches at least the minimum match ( $m_{\text{eff}} \geq 0.97$ ). We store the number of components for each template in our bank.

#### E. Search Pipeline and Coincidence Analysis

We use the harmonic search implementation [45] in the open-source software PyCBC [54] to perform

our precessing search. We restrict the number of harmonics to three to have a good compromise between the increasing computational costs of matched filtering and the ability to capture precessional effects from the data. We matched filter single detector data using the number of harmonics associated with each template to get SNR time-series for each harmonic. Then we add each harmonic SNR series in quadrature to the complete SNR time-series for the corresponding template.

To mitigate the effect of non-Gaussian noise artifacts, we perform two non-Gaussian vetoing tests: a modified version of the  $\chi^2$  test (as implemented in [45]) and an optimized version of the sine-Gaussian  $\chi^2$  test [55] (discussed in the next section). The standard  $\chi^2$  test checks for differences in the expected and computed power in different frequency bands. For our precessing search, we compute the expected power for a reconstructed signal from a trigger. The reconstructed signal is a combination of the harmonics (up to three) weighted by their respective SNRs. Furthermore, we use the PSD variation statistics to incorporate short-term PSD variability [56]. The SNR,  $\chi^2$ , sine-Gaussian and PSD variation statistics are combined together to rank the triggers from a single detector.

We then perform a coincident search between data from the two detectors – LIGO Hanford and LIGO Livingston and use the multi-detector ranking statistic implemented in [45]. The ranking statistic is constructed using the allowed coincidence window between detectors, the expected noise-rate density, and the likelihoods of extrinsic parameters under the signal and noise hypotheses. These likelihoods are derived by comparing the amplitudes and phases of a single harmonic across detectors, ensuring both share the same  $b_k$  value, thereby removing dependence on intrinsic template parameters. The harmonic with the highest signal-to-noise ratio serves as the reference for evaluating amplitude ratio, phase difference, and time difference relative to the second detector.

For our aligned-spin search, we use the same search configuration and ranking statistic as used for the PyCBC analysis of the O3 data for producing the GWTC-3 catalog [22]. The aligned-spin search ranking statistic is further enhanced by incorporating an additional KDE-based statistic, which accurately models the probability distributions of binary source parameters across the template bank [57].

## F. Improvements to the Harmonic Search

The previous scheme to compute the harmonics works naturally for templates that have  $b < 1$ : in the *original* harmonic order with  $h_0$  being the dominant harmonic. However, this is not true for  $b \geq 1$ : since the harmonic amplitudes scale roughly with  $b^k$  as the harmonic order is *reversed*, the fifth harmonic will have the dominant contribution followed by the fourth, third and so on. The

effective match with the original harmonics for  $b \geq 1$  templates is greater than the minimum match only when the later harmonics are included. The original harmonic order may lead to a larger number of harmonics than the reversed order and therefore, is not effective for  $b \geq 1$  systems.

One way to obtain harmonics for  $b \geq 1$  systems is to change the harmonic expansion in terms of  $b^{-1} = \cot(\beta/2)$  [41]. In this work, we implement an easier solution and that is to simply reverse the harmonic order at  $b = 1$ . Therefore, depending on the  $b$  value for a template, we use the following *new* order of the harmonics:

$$\text{for } b < 1 : [h_0, h_1, h_2, h_3, h_4] \quad (22)$$

$$b \geq 1 : [h_4, h_3, h_2, h_1, h_0]. \quad (23)$$

We perform the orthogonalization procedure (equation 21) only after reversing the harmonics, as this ensures maximum variance is captured on the first step. Once the new orthogonalized harmonics are obtained for templates with  $b \geq 1$ , we perform the matched filtering as previously described. We additionally employ an improved version of the IMRPhenomXP waveform model to reduce the number of harmonics required for approximately  $\sim 2.5\%$  of templates that exhibit unphysical features. This issue and the corresponding modifications are discussed in detail in the Appendix A.

Figure 3 shows the number of harmonics assigned to each template in the mass-ratio  $q = m_1/m_2$  and  $b$  space for both the original and the updated harmonic prescriptions. With the new scheme, 35,461 templates require fewer harmonics than before. Only for systems close to  $b \sim 1$  multiple harmonics are needed. Reordering the harmonic assignment, we reduce the total number of filters by 65,355, and the number of templates requiring five harmonics drops from 29,580 to just 3. Reversing the harmonics helps massively to improve the efficiency of our search, and the improvement comes in fact with reduced computational costs. The broader implications of this refinement—particularly its impact on the fitting factors and overall search performance—will be explored in the next section.

We also introduce improvements to the efficiency of the sine-Gaussian  $\chi^2$  test. In our precessing search, short-duration noise transients (“blips”) frequently produce triggers that require repeated evaluation of the sine-Gaussian  $\chi^2$  veto. This leads to a substantial computational burden, particularly in regions of parameter space where blip rates are high. To mitigate this, we implemented optimizations that reduce the cost of computing the sine-Gaussian  $\chi^2$  without altering its discriminatory power. These enhancements make the veto significantly faster, improving the overall throughput of the search while maintaining robust rejection of non-Gaussian noise.

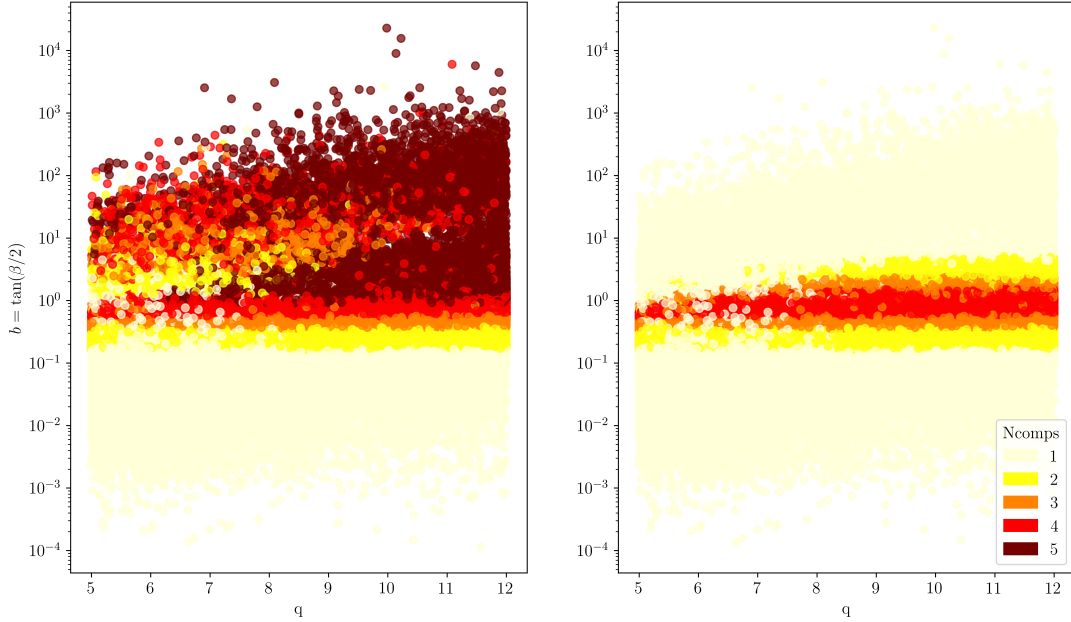


FIG. 3. The number of harmonics required by every template in our bank as represented by the  $(q, b)$  parameter space, where  $q = m_1/m_2$ . We show the number of harmonics obtained using the original harmonic order  $[h_0, h_1, h_2, h_3, h_4]$  (left), and using the new harmonic order (reversed order for  $b \geq 1$ ) (right). The color of each point represents the number of required harmonics: darker templates require more harmonics and lighter the fewer (see legend). Notice the significant reduction in the number of harmonics in the upper region ( $b \gtrsim 1$ ) from left to right plot: a total of 35461 templates have fewer harmonics on the with the new harmonic scheme. By incorporating the new harmonic order, the total number of harmonics for the entire bank is reduced by 65355, and the number of templates requiring 5 harmonics reduces from 29580 to only 3. Comparing the total number of filters to the previous preprocessing BBH search [33, 39], we have five times fewer filters.

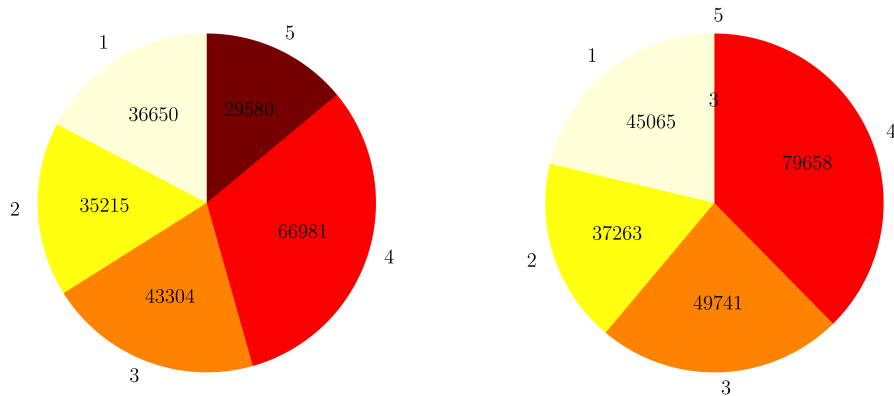


FIG. 4. Pie chart of the templates grouped according to their required number of harmonics (denoted by the numbers inside the pie). On the left is the distribution with the original harmonics, and on the right is the distribution with the new harmonic order where we apply the reverse harmonic order for  $b \geq 1$  templates. Improving to the new scheme, 35461 templates have fewer harmonics. Summing up the numbers in each pie, we find there are in total 65355 additional number of harmonics (filters) with the original harmonic order. With the new scheme the number of templates requiring five harmonics reduces from 29580 to 3.

Parameter	Range	Distribution	
$m_1$	$[15, 70]M_\odot$	Uniform	
$m_2$	$[3, 10]M_\odot$	Uniform	
$q$	$[5, 12]$	Constraint on the masses	
Spin-directions	$[0, \pi]$	Isotropic	
$\phi_c$	$[0, 2\pi]$	Uniform angle	
$i$	$[0, \pi]$	Uniform in sin angle	
$(\alpha, \delta)$	$([0, 2\pi], [0, \pi])$	Uniform sky	
$\psi$	$[0, 2\pi]$	Uniform	
$d_L^c$	$[30, 350]$ Mpc	Uniform	
	Parameter	Range	Distribution
Highly-precessing	$ s_1 $	$[0.0, 0.99]$	Uniform in $ s_1 ^4$
	$ s_2 $	$[0.0, 0.99]$	Uniform in $ s_2 ^4$
Normal-precessing	$ s_1 $	$[0.0, 0.99]$	Uniform in $ s_1 $
	$ s_2 $	$[0.0, 0.99]$	Uniform in $ s_2 $

TABLE II. Description of the *highly precessing* injected population of signals (same as the one used in [33]). We also generate a *normal precessing* injection population that is sampled from the above except the spin magnitudes are distributed uniformly in the first power between the range  $[0.0, 0.99]$ .

### III. ASSESSING THE VALIDITY OF OUR SEARCH METHOD

#### A. Validity of our template bank

We test the validity of our template bank by checking the fitting factors obtained for a population of simulated binaries. For a faithful comparison of the efficiency of our bank with the bank used in the study [33], we use the same distributions to sample the binary parameters. The prior ranges correspond to the same masses and extrinsic parameters as in Table I but with different priors on the spin magnitude. In [33], nonphysical priors of uniform in the fourth power of  $|s|^4$  were used to make sure a large fraction of the population corresponds to highly precessing systems. In addition to the nonphysical prior, we employ the standard astrophysical prior of uniform in the first power  $|s|$  of the spin magnitudes. The prior distributions for both our injected population are described in Table II.

We compute the fitting factors for highly precessing injections using up to three harmonics. In the Figure 5 we show the cumulative distribution function of the fitting factors obtained via three different banks: 1) bank used in the previous precessing search [33, 39], 2) our bank with the original harmonic order, 3) our bank including the reverse harmonic order. Our bank with either of the harmonic order produces better fitting factors than the bank in [33]. With the new harmonic order fitting factors are better than the original harmonics. We also show the fitting factor distribution when choosing different maximum number of harmonics in Figure 6. The fitting factors improve further if including the fourth and the fifth harmonic. However, currently the ranking statistic used in our search is defined only for up to three

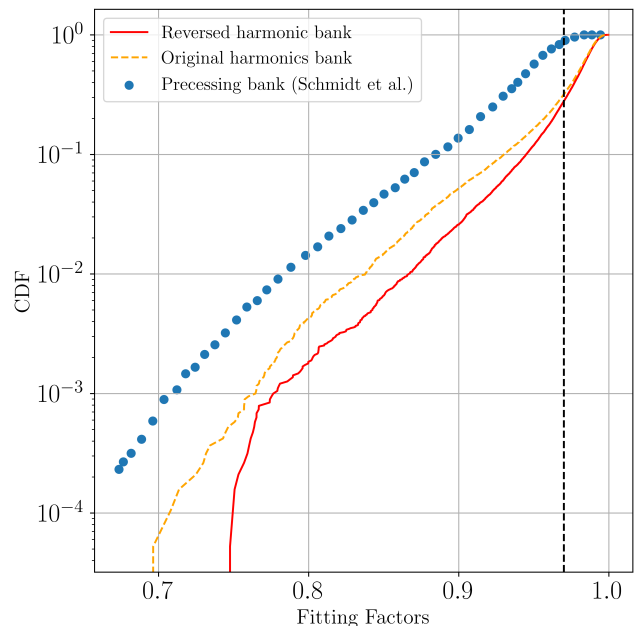


FIG. 5. Cumulative distribution of fitting factors for the highly precessing injection set (as described in Table II) obtained by the previous precessing BBH search bank (blue circles) [33], by our harmonic bank with original harmonics order (orange dotted line) and the same bank including the new harmonic order (red bold line). The previous precessing search bank contains  $\sim 2.3 \times 10^6$  and our bank contains  $\sim 2 \times 10^5$  templates. Our bank achieves much better fitting factors with  $5 \times$  fewer filters compared to the previous search, after accounting for the extra harmonics for each template (up to three). The black-dotted line corresponds to the minimum match of the bank = 0.97.

harmonics.

#### B. Evaluating search sensitivity via Monte-Carlo integration

A search pipeline's efficiency is quantified by its ability to recover a population of simulated signals embedded in the data. This efficiency is expressed in terms of the sensitive space-time volume,  $\langle VT \rangle$ , which characterizes the fiducial volume within which the pipeline can detect signals over an observation time  $T_{\text{obs}}$ . The population-averaged sensitive space-time volume is defined as:

$$\langle VT \rangle = T_{\text{obs}} \int \int p(z, \zeta | \text{FAR}) \frac{dV_c}{dz} \frac{1}{1+z} dz d\zeta, \quad (24)$$

where  $dV_c/dz$  is the differential co-moving volume and  $p(z, \zeta | \text{FAR})$  is the detection probability of detecting a binary system with  $\zeta$  parameters at a redshift  $z$  given a FAR threshold.

Signals are injected into the detector data and then recovered using a search pipeline. However, if an

TABLE III. This table lists the 29 GWTC events recovered by our combined search with an inverse FAR greater than 1 per year. For each recovered event, we present the GPS time, the IFAR [Yr] obtained by the PyCBC-BBH analysis in the GWTC-2.1 [58] or GWTC-3 [22] catalogs, and the IFAR [Yr] obtained by our combined search. In the combined search, we assign equal weight to the aligned-spin and precessing-only searches; consequently, the reported IFAR corresponds to the mean of the two sub-search IFARs.

Event	GPS time	GWTC PyCBC IFAR [Yr]	Our combined search IFAR [Yr]
GW190408_181802	1238782700.28	$8.3 \times 10^3$	$2.7 \times 10^4$
GW190412_053044	1239082262.17	$8.3 \times 10^3$	$8.0 \times 10^3$
GW190503_185404	1240944862.29	384.6	10.0
GW190512_180714	1241719652.42	$9.1 \times 10^3$	$4.4 \times 10^3$
GW190519_153544	1242315362.40	$9.0 \times 10^3$	4.1
GW190521_030229	1242442967.46	769.2	1.8
GW190521_074359	1242459857.46	$4.4 \times 10^4$	$5.6 \times 10^4$
GW190706_222641	1246487219.34	2.9	96.5
GW190707_093326	1246527224.17	$5.3 \times 10^4$	$7.6 \times 10^4$
GW190720_000836	1247616534.70	$1.3 \times 10^4$	$1.2 \times 10^4$
GW190725_174728	1248112066.46	0.3	3.3
GW190727_060333	1248242631.98	$5 \times 10^3$	4.1
GW190728_064510	1248331528.53	$1.3 \times 10^4$	$3.2 \times 10^4$
GW190828_063405	1251009263.75	$1.4 \times 10^4$	$3.6 \times 10^4$
GW190828_065509	1251010527.88	$9.0 \times 10^3$	510.5
GW190915_235702	1252627040.69	$1.4 \times 10^4$	$6.0 \times 10^2$
GW190924_021846	1253326744.84	$1.2 \times 10^4$	600
GW190930_133541	1253885759.24	83.3	20.5
GW191105_143521	1256999739.93	27.8	103.8
GW191109_010717	1257296855.22	21.3	7.2
GW191129_134029	1259070047.20	$4.2 \times 10^4$	$3.8 \times 10^4$
GW191204_171526	1259514944.09	$8.3 \times 10^4$	$7.0 \times 10^4$
GW191215_223052	1260484270.33	3.6	126.9
GW191222_033537	1261020955.12	$1.0 \times 10^4$	4.2
GW200128_022011	1264213229.89	232.5	1.1
GW200224_222234	1266618172.40	$1.3 \times 10^4$	$4.8 \times 10^4$
GW200225_060421	1266645879.39	$2.4 \times 10^4$	$1.5 \times 10^4$
GW200311_115853	1267963151.39	$1.3 \times 10^4$	$3.7 \times 10^4$
GW200316_215756	1268431094.16	1.72	48.0

astrophysical distribution is used, then a large fraction of injections are not recoverable by any searches since they are placed at distances greater than the reach of current detectors, which leads to poor estimation of the detection probability  $p_{\text{inj}}(z, \zeta)$ . Therefore, we use a prior that allows better estimation of the detection probability, and then re-weight the above integral to an astrophysical distribution according to the method described in [59].

We sample the chirp-distance  $d_L^c = \mathcal{M}_c^{5/6} d_L$  uniformly such that lighter (quieter) systems are placed closer and heavier (louder) systems are placed further away. Also, the mass distributions are chosen uniformly for convenience. The weights are written as the ratio of the probabilities of the astrophysical  $p_{\text{astro}}$  and injected  $p_{\text{inj}}$  distance (chirp-distance) distributions as:

$$w_i = \frac{p_{\text{astro}}(d_L^c[i])}{p_{\text{inj}}(d_L^c[i])}, \quad (25)$$

$$= p_{\text{astro}}(d_L[i]) \times (\mathcal{M}_c[i])^{5/6} \quad (26)$$

$$= p_{\text{astro}}(d_c[i]) \times (1 + z[i]) \times (\mathcal{M}_c[i])^{5/6}, \quad (27)$$

where  $(\mathcal{M}_c)^{5/6}$  and  $(1 + z)$  factors are the Jacobians for changing the variables from chirp-distance to luminosity distance and then to co-moving distance  $d_c$  ( $d_L^c \rightarrow d_L \rightarrow d_c$ ) respectively. For the target astrophysical distribution, we assume the standard prior of uniform in comoving volume which corresponds to  $p_{\text{astro}}(d_c) \propto d_c^2$ .

Following [59], the Monte-Carlo integration of the equation (24) over the discrete injections is given by

$$\langle VT \rangle = V_c[z_{\text{max}}^{\text{inj}}] \times \frac{\sum_{i \in \text{recovered}} \epsilon[\zeta_i] w_i}{\sum_{i \in \text{all}} \epsilon[\zeta_i] w_i}, \quad (28)$$

where  $\epsilon[\zeta]$  for an injection with  $\zeta$  parameters is either 0 (missed) or 1 (recovered) at a given false alarm rate threshold, and  $V_c[z_{\text{max}}^{\text{inj}}]$  is the co-moving volume up to the maximum redshift  $z_{\text{max}}$  corresponding to the farthest injection in the population

$$V_c[z_{\text{max}}^{\text{inj}}] = \int_0^{z_{\text{max}}} \frac{dV_c}{dz} \frac{1}{1+z} dz. \quad (29)$$

## A. Observational results

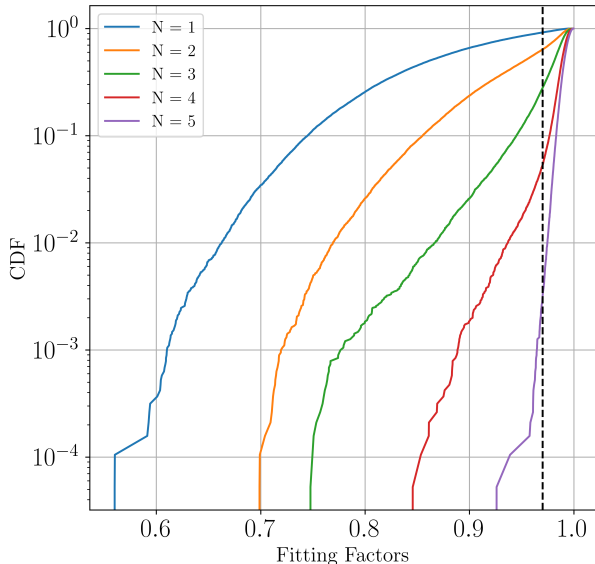


FIG. 6. Cumulative distribution of fitting factors for the highly-precessing population of simulated signals (see Table II) obtained using our template bank (with reverse harmonics included). The different curves represent the fitting factor distributions for using the maximum number of harmonics up to the labeled number (legend). Note, the bank becomes more efficient as we employ more harmonics: as evident by decreasing tail of low fitting factors as the number of harmonics increases. In this search we use only up to three harmonics (green curve). The black-dotted line corresponds to the minimum match of the bank = 0.97.

## IV. SEARCH RESULTS FROM O3 DATA

We search for the publicly available data from the Advanced LIGO detectors during their third observing run [44]. This observing run was split in two runs O3a lasting six-months from April 1st to October 1st 2019, and O3b with five-months from November 1st 2019 to March 27th 2020.

We perform matched filtering with a low-frequency cutoff of 30 Hz. We conduct two searches — a precessing search and an aligned-spin search—using the template banks described previously. For each search, we inject two sets of signals, the highly precessing and normally precessing systems, as listed in Table II. We then combine the results from the individual sub-searches with equal weighting to obtain the results for our *combined* search. The list of top candidates, the template parameters associated with each candidate, and the configuration files necessary to reproduce the analysis are available in our data release [60].

In Table III, we report the list of significant events observed in our search with an inverse FAR greater than 1 per year. We did not find any new events. Our combined search recovered 29 events which were already reported in the previous GWTC catalogs [19, 22, 58]. We miss the GW200129\_065458 event because this event has detector-frame parameters that lie outside our search region.

We also report two sub-threshold ( $\text{IFAR} < 1$  [Yr]) events that were not reported in any GWTC catalogs in Table IV.

## B. Search sensitivity

Aligned-spin searches are always performed, even in highly precessing regions (as the one explored in this work) where they are expected to have reduced sensitivity. Therefore, we explore the efficacy of performing a *combined* search, which is formed by equally combining aligned-spin and precessing search sensitivities. We estimate the improvement in  $\langle VT \rangle$  for our combined search and compare it to our aligned-spin only search. We estimate the sensitivity for each search as described by equation (28). For an aligned-spin search we use an IFAR threshold of 1 per year or above. Since we are searching over the same data twice in the combined search, we must penalize the significances for each sub-search with a trials factor of two, and therefore, apply an IFAR threshold of 2 [Yr] for each sub-search. This effectively makes the combined search IFAR threshold the same as the aligned-spin only search. The sensitivity ratio is computed as

$$\langle VT \rangle_{\text{ratio}} = \frac{\langle VT \rangle_{\text{AS}}^{\text{IFAR} \geq 2} + \langle VT \rangle_{\text{Precessing}}^{\text{IFAR} \geq 2}}{\langle VT \rangle_{\text{AS}}^{\text{IFAR} \geq 1}} \quad (30)$$

In Figure 7, we show the  $\langle VT \rangle_{\text{ratio}}$  for both the 1) highly and 2) normal precessing injection sets (as described in Table II). Our combined search performs consistently better than the aligned-spin-only search. In particular, we observe a gain in sensitivity of up to 28% for highly precessing systems with  $\chi_P \geq 0.5$ . This improvement arises because the aligned-spin search loses sensitivity in these regions, whereas the precessing search maintains robust performance. For weakly precessing systems with  $\chi_P < 0.2$ , the combined search performs on par with the aligned-spin-only search, with only a modest (less than  $\sim 4\%$ ) decrease in sensitivity for aligned-spin injections. Overall, these results demonstrate that our combined strategy delivers a significant enhancement in sensitivity, especially in the regime where precession effects are strong.

TABLE IV. The table lists two candidates from our combined search that have not been previously reported in any GWTC catalogs. For each candidate, we present the parameters from the precessing template yielding the highest ranking statistic. These parameters include the component masses ( $m_1, m_2$ ), spin projections along the orbital angular momentum ( $s_{1z}, s_{2z}$ ), the effective spin  $\chi_{\text{eff}}$ , effective precession parameter  $\chi_P$ . We also provide the matched-filter signal-to-noise ratios measured in LIGO Hanford  $\rho_H$  and LIGO Livingston  $\rho_L$ .

	GPS time	IFAR [yr]	$m_1 [M_\odot]$	$m_2 [M_\odot]$	$s_{1z}$	$s_{2z}$	$\chi_{\text{eff}}$	$\chi_P$	$\rho_H$	$\rho_L$
1	1243736409.19	0.365	40.82	4.31	0.64	0.02	0.58	0.60	5.71	9.02
2	1253413448.93	0.125	35.42	3.02	-0.05	0.02	-0.08	0.53	6.89	7.28

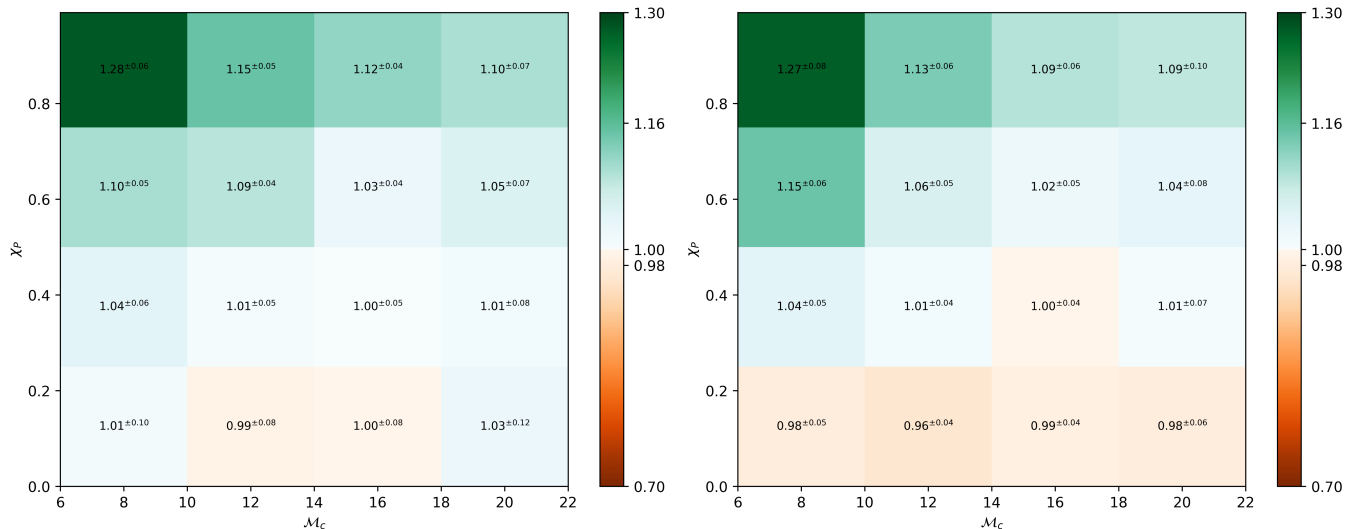


FIG. 7. Ratio of the sensitive  $\langle VT \rangle$ , for a combined (precessing + aligned-spin) search at IFAR threshold of 2.0 [Yr] versus the aligned-spin search at IFAR threshold of 1.0 [Yr] for the *highly precessing* injection set (left) and for *normal precessing* injection set (right). We show the  $(VT)_{\text{ratio}}$  as a function of  $(M_c, \chi_P)$ . We find an overall improvement across the parameter space, with the combined search being up to  $\sim 28\%$  more sensitive compared to an aligned-spin search only. The combined search becomes effective with increasing precessional effects (increasing  $\chi_P$ ) and, with decreasing chirp mass because precessional effects are better measured for longer duration (i.e. smaller chirp mass) signals.

## V. CONCLUSIONS AND FUTURE IMPROVEMENTS

In this work, we apply an improved implementation of the harmonic decomposition technique to carry out a full-scale search for precessing binary black holes in the O3 data of the Advanced LIGO detectors. We introduce a novel method for estimating the number of harmonics, which substantially reduces the number of filters required in a harmonic search. Combined with our template bank, this scheme reduces the filter count by a factor of five relative to the previous search for highly precessing binaries [39], while simultaneously achieving better fitting factors.

We searched over the entire O3 data of Advanced LIGO detectors and found no new significant events. With our precessing search, we have found 29 previously reported events in the latest GWTC-4 catalog [19]. Recognizing that aligned-spin searches will continue to be used as standard searches to produce GW catalogs, we quantify the benefit of a joint search that weights

precessing and aligned-spin searches equally. Relative to an aligned-spin-only search, our combined search improves the sensitive volume by up to 28% for systems with  $\chi_P \geq 0.5$ , and yields more modest gains across the rest of the parameter space.

Aligned-spin searches are highly optimized, no precessing search has developed a ranking statistic that outperforms the performance of aligned-spin searches employed to produce gravitational-wave catalogs. There are two major improvements that can improve the sensitivity of our harmonic search. First, developing a better  $\chi^2$  statistic to better distinguish precessing BBH signals from short-duration (blip) glitches. Our current implementation checks for expected power in the signal which increases as the binary approaches merger. However, precessing templates can have modulations such that they have a significant power away from merger or no power at all close to the merger. We have observed in our search, such templates trigger a large number of high SNR false alarms which contaminate our background estimation and reduce the sensitivity of our search. The glitch classes responsible for the

increased rate of noise triggers in the precessing search are discussed in Appendix B. Implementing a novel  $\chi^2$  method is therefore crucial for improving precessing searches in the future.

Secondly, improving the multi-detector ranking statistic. There are multiple components to enhance this statistic a few of which have already been proposed (but not yet implemented) in [45]. In addition, the phase-time-amplitude histograms required for the ranking statistic, can be extended to include the  $b$  parameter to properly account for the uncertainty due to noise. Addition of a new parameter exponentially increases the phase-time-amplitude file sizes, which may pose computational challenges. Novel methods which can easily and accurately learn the distribution of triggers for a population of astrophysical sources for different detector networks would be needed to extend our current implementation.

Would further enhancing the fitting factors significantly improve the ranking of real precessing events at a given false alarm rate? With the exception of only three templates, the entire template bank satisfies the required number of harmonics. The inclusion of the fourth harmonic leads to a significant improvement in the fitting factors (see Figure 6). However, adding an additional harmonic also increases the degrees of freedom of the matched-filter statistic by two, which in turn leads to a higher false alarm rate. It is therefore worth investigating how the combined search performs when the fourth harmonic is included in a precessing search.

The continued growth of the gravitational-wave event catalog is expected to enhance the prospects of detecting precessing binary systems. Accurate measurement of spin precession will play a crucial role in disentangling the various astrophysical formation channels contributing to the observed population. Given that our combined search has approximately up to 28% greater sensitivity relative to current aligned-spin searches and achieves up to a fivefold improvement in efficiency over existing precessing search methods, it provides a promising framework for future searches for precessing binaries in upcoming gravitational-wave data.

## ACKNOWLEDGMENTS

The authors would like to thank Charlie Hoy and Laura Nuttall for continued discussion throughout this project. We are grateful for the computational resources provided by LIGO Laboratory and the ICG, SEPNet and the University of Portsmouth. This research has made use of data, software and/or web tools obtained from the Gravitational Wave Open Science Center (<https://www.gw-openscience.org>), a service of LIGO Laboratory, the LIGO Scientific Collaboration, the Virgo Collaboration, and KAGRA. This material is based upon work supported by NSF’s LIGO Laboratory,

which is a major facility fully funded by the National Science Foundation. LIGO Laboratory and Advanced LIGO are funded by the United States National Science Foundation (NSF) as well as the Science and Technology Facilities Council (STFC) of the United Kingdom, the Max-Planck-Society (MPS), and the State of Niedersachsen/Germany for support of the construction of Advanced LIGO and construction and operation of the GEO600 detector. The Australian Research Council provided additional support for Advanced LIGO. Virgo is funded through the European Gravitational Observatory (EGO), by the French Centre National de Recherche Scientifique (CNRS), the Italian Istituto Nazionale di Fisica Nucleare (INFN) and the Dutch Nikhef, with contributions by institutions from Belgium, Germany, Greece, Hungary, Ireland, Japan, Monaco, Poland, Portugal, Spain. KAGRA is supported by the Ministry of Education, Culture, Sports, Science and Technology (MEXT), Japan Society for the Promotion of Science (JSPS) in Japan; National Research Foundation (NRF) and the Ministry of Science and ICT (MSIT) in Korea; Academia Sinica (AS) and National Science and Technology Council (NSTC) in Taiwan.

## Appendix A: Unphysical features in IMRPhenomXP

We find that for 4980 ( $\sim 2.5\%$ ) templates in our bank, the default prescription of the IMRPhenomXP waveform model shows unphysical sharp kinks in the frequency domain waveforms. An example of this is shown in Figure 8. The harmonic decomposition of the templates is not an accurate representation of a physical system. In such cases, the harmonics peak in amplitude around the sharp kinks to fit the waveform better, and therefore, all five harmonics are required to reconstruct such unphysical templates. These unphysical features penalize our search in two ways: 1) they lead to more than required number of filters, and 2) the sub-dominant harmonics match with glitches, causing higher rate of false alarms.

We attribute these kinks to the use of the default prescription for the Euler angles. By default, the next-to-next-to-leading-order (NNLO) prescription is employed to map aligned-spin waveform modes in the co-precessing frame to precessing waveform modes in the inertial frame, as described in [61]. However, previous studies have shown that the NNLO prescription fails to accurately capture complex precessional dynamics, such as transitional precession [62]. We find that this limitation affects a significant portion of our search parameter space, leading to unphysical features in some templates. To address this issue, we adopt the more accurate, albeit slightly slower, SpinTaylor prescription for the Euler angles [63], which successfully removes these unphysical features (see also Figure 8). The SpinTaylor implementation of IMRPhenomXP is at most a factor of four slower than the default NNLO version.

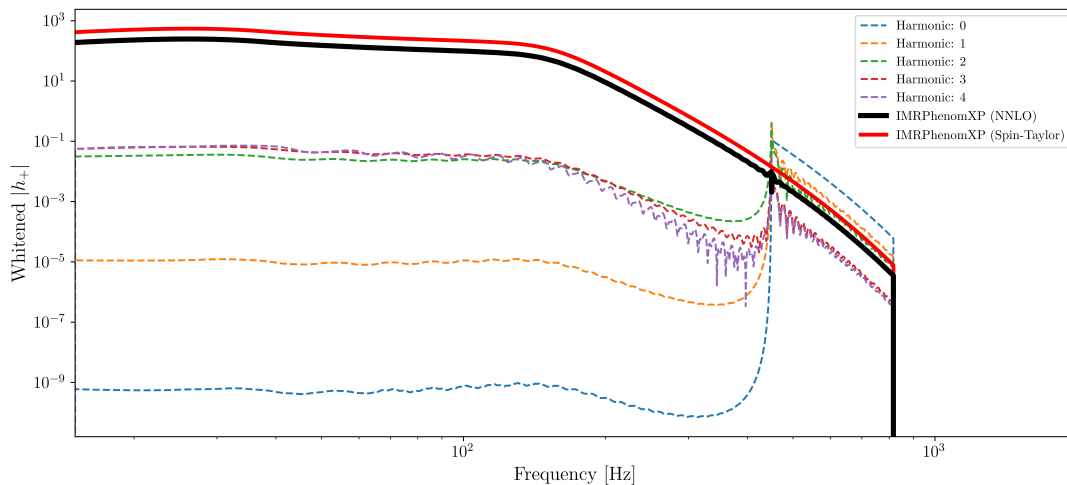


FIG. 8. Example of an unphysical feature observed when using the default IMRPhenomXP (NNLO angles) waveform model (black bold line). The waveform corresponds to the system with intrinsic parameters:  $(m_1, m_2) = (68.11, 6.462)$ , and spins  $\vec{s}_1 \simeq [0.0, 0.0, -0.85]$ ,  $\vec{s}_2 \simeq [0.04, 0.02, -0.44]$ . The sharp kink observed around  $\sim 400$  Hz forces all the harmonics (dashed lines) to increase in amplitude to fit the unphysical feature better – the number of harmonics required in such cases is always five. When using the more accurate SpinTaylor prescription for the same approximant, the kink disappears (red bold line). The harmonics corresponding to the improved waveform model (not shown) do not peak close to the kink.

## Appendix B: Increased rate of background triggers

Our precessing search has a higher rate of noise (background) triggers than for the aligned-spin search. The additional degrees of freedom in the single-detector ranking statistic raise the noise floor, leading to a huge number of noise triggers surviving the vetoing and coincidence steps. As a result, the precessing search is more susceptible to producing loud coincident noise events than the aligned-spin search as shown in Figure 9. The coincident ranking statistics for the two searches are different, which prevents a direct quantitative comparison along the horizontal axes, however, a clear qualitative distinction is observed in the vertical axes and the tails of the distributions. The precessing search shows a pronounced excess of high-ranking noise triggers, corresponding to an elevated false-alarm rate at large statistic values.

A further contribution to the elevated false-alarm rate in the precessing search arises from the limited effectiveness of the current signal-consistency (chi-squared) tests in suppressing certain classes of instrumental glitches. We find there are two classes of glitches that severely impact the sensitivity of our search: 1) *blip* glitches 2) *scattering* glitches. Short-duration templates, such as those corresponding to highly asymmetric, high-mass and/or highly-precessing systems, can closely match blip glitches, with significant signal power as shown in Figure 10. In Figures 10 and 11, we show template corresponding to a highly asymmetrical and highly spinning source that matched with different class of glitches leading to a coincident trigger that contaminated our background. Due to the

extremely short duration ( power confined to the final  $\sim 0.01$  s of the waveform) of the template in Hanford, the chi-squared test struggle to sufficiently penalize such triggers in individual detectors. We also find, templates with substantial power away from the merger can couple strongly to low-frequency scattering noise (shown in Figure 11). Since the present chi-squared implementation primarily tests for increasing power with increasing gravitational-wave frequency, it is not optimally designed to down-rank triggers dominated by pre-merger or low-frequency power. Together, these effects lead to an accumulation of high-ranking noise triggers and highlight key limitations of the current veto strategy in the presence of instrumental artifacts.

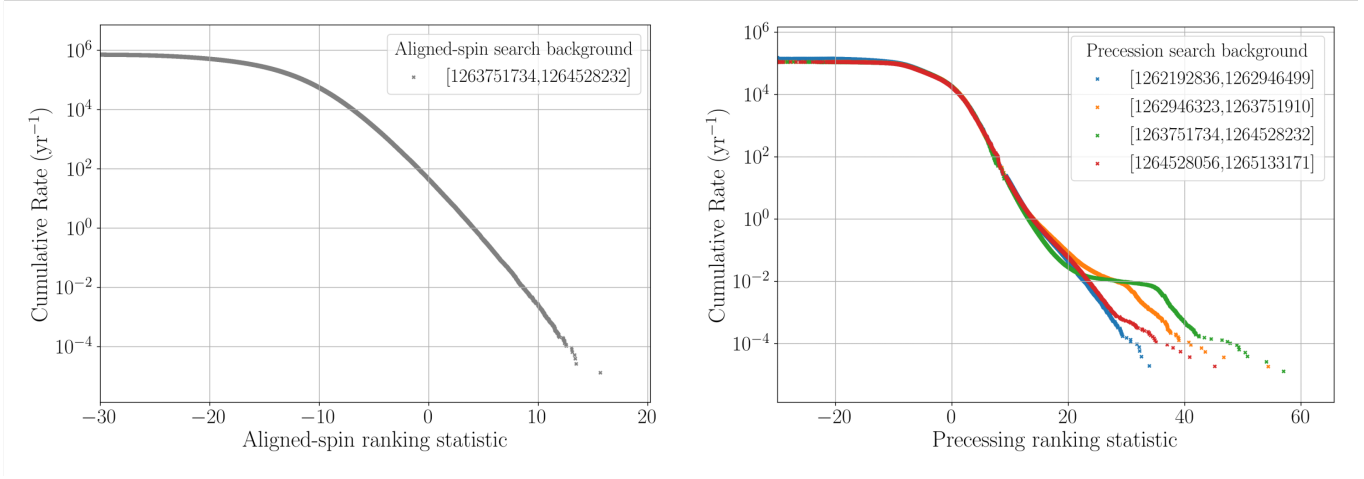


FIG. 9. Background distributions of coincident (HL) ranking statistics for noise triggers in the aligned-spin (left) and precessing (right) searches. The vertical axis shows the false-alarm rate, while the horizontal axes show the coincident ranking statistics used in each search. Because the two searches use different ranking statistics, we do not make a direct quantitative comparison between them. Qualitatively, the precessing search exhibits a higher rate of noise triggers. This behavior arises from the increased degrees of freedom in the precessing single-detector ranking statistic, which raises the effective noise floor. For the aligned-spin search, the cumulative background—shown for GPS times [1263751734, 1264528232]—falls off exponentially with increasing ranking statistic and remains consistent throughout the O3 run. In contrast, the precessing search shows extended background tails during periods of increased glitch rates. We show the background distribution over four data chunks. Note the indicated kinks in the green and orange curves. These kinks arise from glitches such as blips and scattered-light noise that the current implementation of the  $\chi^2$  tests does not effectively down-rank, leading to an excess of high-ranking noise triggers and an increased false-alarm rate.

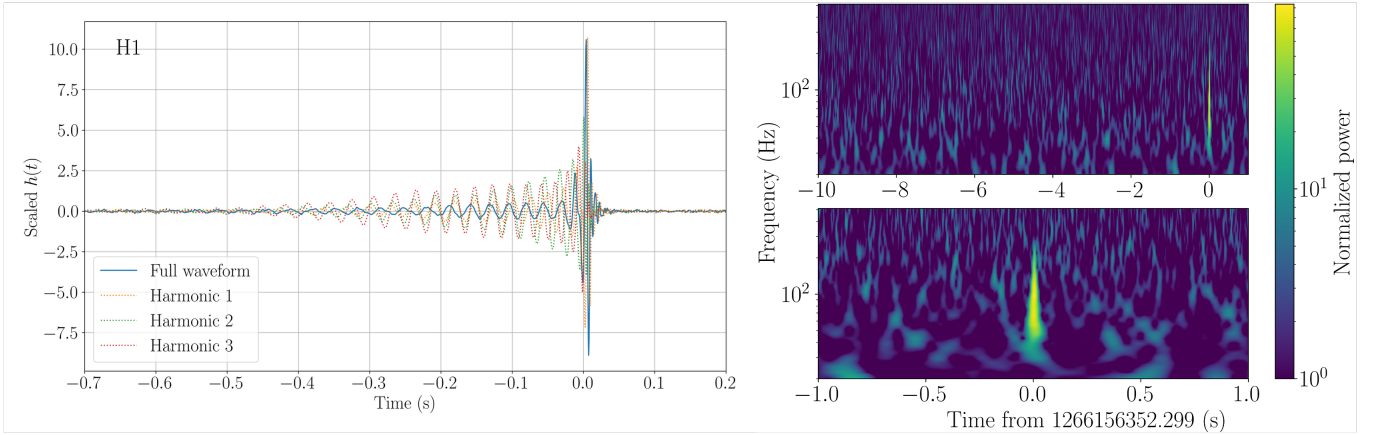


FIG. 10. Example of an extremely short duration template triggering a blip glitch in LIGO Hanford. The template corresponds to highly-asymmetrical  $(m_1^{\text{det}}, m_2^{\text{det}}) = (59, 5)M_\odot$  source. Significant power in the signal is only during the last  $\sim 0.01$  second which matches the blip glitch as visible in the spectrograms (second column). Since the template is extremely short duration, our current chi-squared tests struggle to penalize such single detector triggers.

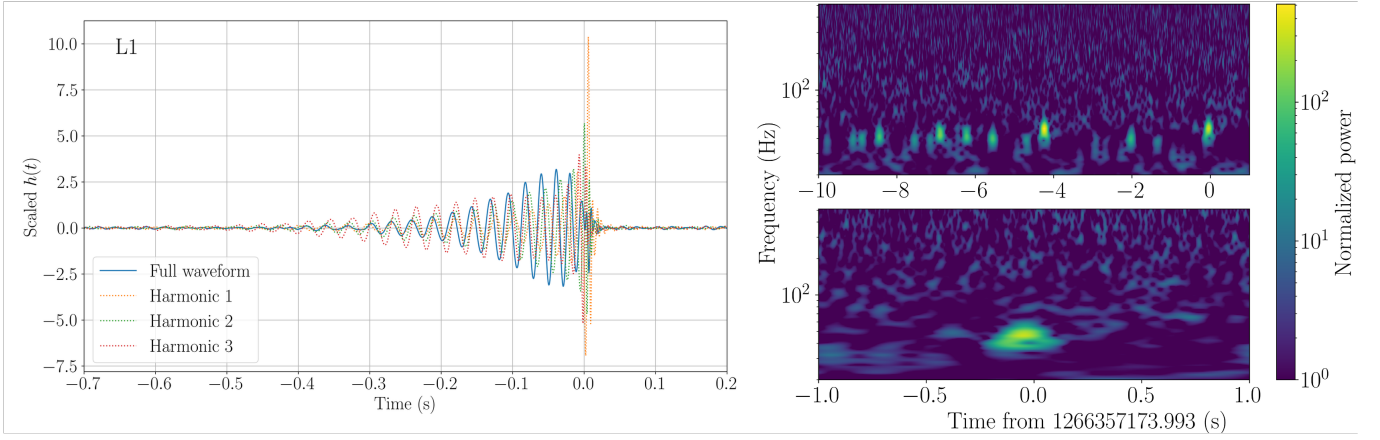


FIG. 11. Example of a template that exhibits significant power away from the merger. This template is identical to the one shown in Figure 10 and corresponds to a highly asymmetric source with detector-frame masses  $(m_1^{\text{det}}, m_2^{\text{det}}) = (59, 5), M_\odot$ . Such templates typically match low-frequency scattering noise. Because the current implementation of the  $\chi^2$  test is designed to identify increasing power with increasing gravitational-wave frequency, peaking near merger, the search has limited ability to effectively down-rank triggers of this type.

- 
- [1] “GWTC-4.0: Population Properties of Merging Compact Binaries,” (2025), arXiv:2508.18083 [astro-ph.HE].
- [2] Theocharis A. Apostolatos, Curt Cutler, Gerald J. Sussman, and Kip S. Thorne, “Spin induced orbital precession and its modulation of the gravitational wave forms from merging binaries,” *Phys. Rev. D* **49**, 6274–6297 (1994).
- [3] Juan Calderón Bustillo, Pablo Laguna, and Deirdre Shoemaker, “Detectability of gravitational waves from binary black holes: Impact of precession and higher modes,” *Phys. Rev. D* **95**, 104038 (2017), arXiv:1612.02340 [gr-qc].
- [4] Ian Harry, Stephen Privitera, Alejandro Bohé, and Alessandra Buonanno, “Searching for Gravitational Waves from Compact Binaries with Precessing Spins,” *Phys. Rev. D* **94**, 024012 (2016), arXiv:1603.02444 [gr-qc].
- [5] Geraint Pratten, Patricia Schmidt, Riccardo Buscicchio, and Lucy M. Thomas, “Measuring precession in asymmetric compact binaries,” *Phys. Rev. Res.* **2**, 043096 (2020), arXiv:2006.16153 [gr-qc].
- [6] Rhys Green, Charlie Hoy, Stephen Fairhurst, Mark Hannam, Francesco Pannarale, and Cory Thomas, “Identifying when Precession can be Measured in Gravitational Waveforms,” *Phys. Rev. D* **103**, 124023 (2021), arXiv:2010.04131 [gr-qc].
- [7] Ilya Mandel and Alison Farmer, “Merging stellar-mass binary black holes,” *Phys. Rept.* **955**, 1–24 (2022), arXiv:1806.05820 [astro-ph.HE].
- [8] Michela Mapelli, “Formation Channels of Single and Binary Stellar-Mass Black Holes,” (2021) arXiv:2106.00699 [astro-ph.HE].
- [9] Davide Gerosa and Maya Fishbach, “Hierarchical mergers of stellar-mass black holes and their gravitational-wave signatures,” *Nature Astron.* **5**, 749–760 (2021), arXiv:2105.03439 [astro-ph.HE].
- [10] Vassiliki Kalogera, “Spin orbit misalignment in close binaries with two compact objects,” *Astrophys. J.* **541**, 319–328 (2000), arXiv:astro-ph/9911417.
- [11] Davide Gerosa, Emanuele Berti, Richard O’Shaughnessy, Krzysztof Belczynski, Michael Kesden, Daniel Wysocki, and Wojciech Gladysz, “Spin orientations of merging black holes formed from the evolution of stellar binaries,” *Phys. Rev. D* **98**, 084036 (2018), arXiv:1808.02491 [astro-ph.HE].
- [12] Krzysztof Belczynski, Alessandra Buonanno, Matteo Cantiello, Chris L. Fryer, Daniel E. Holz, Ilya Mandel, M. Coleman Miller, and Marek Walczak, “The Formation and Gravitational-Wave Detection of Massive Stellar Black-Hole Binaries,” *Astrophys. J.* **789**, 120 (2014), arXiv:1403.0677 [astro-ph.HE].
- [13] Carl L. Rodriguez, Michael Zevin, Chris Pankow, Vassiliki Kalogera, and Frederic A. Rasio, “Illuminating Black Hole Binary Formation Channels with Spins in Advanced LIGO,” *Astrophys. J. Lett.* **832**, L2 (2016), arXiv:1609.05916 [astro-ph.HE].
- [14] R. Abbott *et al.* (KAGRA, VIRGO, LIGO Scientific), “Population of Merging Compact Binaries Inferred Using Gravitational Waves through GWTC-3,” *Phys. Rev. X* **13**, 011048 (2023), arXiv:2111.03634 [astro-ph.HE].
- [15] V. Raymond, M. V. van der Sluys, I. Mandel, V. Kalogera, C. Rover, and N. Christensen, “Degeneracies in Sky Localisation Determination from a Spinning Coalescing Binary through Gravitational Wave Observations: A Markov-Chain Monte-Carlo Analysis for two Detectors,” *Class. Quant. Grav.* **26**, 114007 (2009), arXiv:0812.4302 [gr-qc].
- [16] Qianyun Yun, Wen-Biao Han, Qian Hu, and Haiguang Xu, “Precessing binary black holes as better dark sirens,” *Mon. Not. Roy. Astron. Soc.* **527**, L60–L65 (2023), arXiv:2310.13629 [gr-qc].
- [17] Hengrui Zhu *et al.*, “Black hole spectroscopy for precessing binary black hole coalescences,” *Phys. Rev. D* **111**, 064052 (2025), arXiv:2312.08588 [gr-qc].
- [18] Juan Calderón Bustillo, Adrian del Rio, Nicolas Sanchis-Gual, Koustav Chandra, and Samson H. W. Leong, “Testing Mirror Symmetry in the Universe with LIGO-Virgo Black-Hole Mergers,” *Phys. Rev. Lett.* **134**, 031402 (2025), arXiv:2402.09861 [gr-qc].
- [19] “GWTC-4.0: Updating the Gravitational-Wave Transient Catalog with Observations from the First Part of the Fourth LIGO-Virgo-KAGRA Observing Run,” (2025), arXiv:2508.18082 [gr-qc].
- [20] J. Aasi *et al.* (LIGO Scientific), “Advanced LIGO,” *Class. Quant. Grav.* **32**, 074001 (2015), arXiv:1411.4547 [gr-qc].
- [21] F. Acernese *et al.* (VIRGO), “Advanced Virgo: a second-generation interferometric gravitational wave detector,” *Class. Quant. Grav.* **32**, 024001 (2015), arXiv:1408.3978 [gr-qc].
- [22] R. Abbott *et al.* (KAGRA, LIGO Scientific, VIRGO), “GWTC-3: Compact Binary Coalescences Observed by LIGO and Virgo during the Second Part of the Third Observing Run,” *Phys. Rev. X* **13**, 041039 (2023), arXiv:2111.03606 [gr-qc].
- [23] Patricia Schmidt, Frank Ohme, and Mark Hannam, “Towards models of gravitational waveforms from generic binaries II: Modelling precession effects with a single effective precession parameter,” *Phys. Rev. D* **91**, 024043 (2015), arXiv:1408.1810 [gr-qc].
- [24] Mark Hannam *et al.*, “General-relativistic precession in a black-hole binary,” *Nature* **610**, 652–655 (2022), arXiv:2112.11300 [gr-qc].
- [25] Charlie Hoy, Stephen Fairhurst, and Ilya Mandel, “Rarity of precession and higher-order multipoles in gravitational waves from merging binary black holes,” *Phys. Rev. D* **111**, 023037 (2025), arXiv:2408.03410 [gr-qc].
- [26] Tito Dal Canton *et al.*, “Implementing a search for aligned-spin neutron star-black hole systems with advanced ground based gravitational wave detectors,” *Phys. Rev. D* **90**, 082004 (2014), arXiv:1405.6731 [gr-qc].
- [27] Samantha A. Usman *et al.*, “The PyCBC search for gravitational waves from compact binary coalescence,” *Class. Quant. Grav.* **33**, 215004 (2016), arXiv:1508.02357 [gr-qc].
- [28] Cody Messick *et al.*, “Analysis Framework for the Prompt Discovery of Compact Binary Mergers in Gravitational-wave Data,” *Phys. Rev. D* **95**, 042001 (2017), arXiv:1604.04324 [astro-ph.IM].
- [29] Alexander H. Nitz, Thomas Dent, Tito Dal Canton, Stephen Fairhurst, and Duncan A. Brown, “Detecting binary compact-object mergers with gravitational waves:

- Understanding and Improving the sensitivity of the PyCBC search,” *Astrophys. J.* **849**, 118 (2017), arXiv:1705.01513 [gr-qc].
- [30] Christopher Alléné *et al.*, “The MBTA pipeline for detecting compact binary coalescences in the fourth LIGO-Virgo-KAGRA observing run,” *Class. Quant. Grav.* **42**, 105009 (2025), arXiv:2501.04598 [gr-qc].
- [31] Koustav Chandra, V. Gayathri, Juan Calderon Bustillo, and Archana Pai, “Numerical relativity injection analysis of signals from generically spinning intermediate mass black hole binaries in Advanced LIGO data,” *Phys. Rev. D* **102**, 044035 (2020), arXiv:2002.10666 [astro-ph.CO].
- [32] Rahul Dhurkunde and Alexander H. Nitz, “Sensitivity of spin-aligned searches for neutron star-black hole systems using future detectors,” *Phys. Rev. D* **106**, 103035 (2022), arXiv:2207.14645 [astro-ph.IM].
- [33] Stefano Schmidt *et al.*, “Searching for gravitational-wave signals from precessing black hole binaries with the GstLAL pipeline,” *Phys. Rev. D* **110**, 023038 (2024), arXiv:2403.17186 [gr-qc].
- [34] Alexander H. Nitz, Sumit Kumar, Yi-Fan Wang, Shilpa Kastha, Shichao Wu, Marlin Schäfer, Rahul Dhurkunde, and Collin D. Capano, “4-OGC: Catalog of Gravitational Waves from Compact Binary Mergers,” *Astrophys. J.* **946**, 59 (2023), arXiv:2112.06878 [astro-ph.HE].
- [35] Seth Olsen, Tejaswi Venumadhav, Jonathan Mushkin, Javier Roulet, Barak Zackay, and Matias Zaldarriaga, “New binary black hole mergers in the LIGO-Virgo O3a data,” *Phys. Rev. D* **106**, 043009 (2022), arXiv:2201.02252 [astro-ph.HE].
- [36] A. G. Abac *et al.* (LIGO Scientific, VIRGO, KAGRA), “GWTC-4.0: Methods for Identifying and Characterizing Gravitational-wave Transients,” (2025), arXiv:2508.18081 [gr-qc].
- [37] Philippe Grandclement, Vassiliki Kalogera, and Alberto Vecchio, “Searching for gravitational waves from the inspiral of precessing binary systems: Problems with current waveforms,” *Phys. Rev. D* **67**, 042003 (2003), arXiv:gr-qc/0207062.
- [38] Chris Van Den Broeck, Duncan A. Brown, Thomas Cokelaer, Ian Harry, Gareth Jones, B. S. Sathyaprakash, Hideyuki Tagoshi, and Hirotaka Takahashi, “Template banks to search for compact binaries with spinning components in gravitational wave data,” *Phys. Rev. D* **80**, 024009 (2009), arXiv:0904.1715 [gr-qc].
- [39] Stefano Schmidt *et al.*, “Searching for Asymmetric and Heavily Precessing Binary Black Holes in the Gravitational Wave Data from the LIGO Third Observing Run,” *Phys. Rev. Lett.* **133**, 201401 (2024), arXiv:2406.17832 [gr-qc].
- [40] Ian Harry and Charlie Hoy, “Further constraining the neutron star-black hole merger rate,” (2025), arXiv:2503.09773 [hep-ex].
- [41] Stephen Fairhurst, Rhys Green, Charlie Hoy, Mark Hannam, and Alistair Muir, “Two-harmonic approximation for gravitational waveforms from precessing binaries,” *Phys. Rev. D* **102**, 024055 (2020), arXiv:1908.05707 [gr-qc].
- [42] A. Lundgren and R. O’Shaughnessy, “Single-spin precessing gravitational waveform in closed form,” *Phys. Rev. D* **89**, 044021 (2014), arXiv:1304.3332 [gr-qc].
- [43] R. O’Shaughnessy, Prakash Nepal, and A. Lundgren, “A semianalytic Fisher matrix for precessing binaries with a single significant spin,” *Class. Quant. Grav.* **37**, 115006 (2020), arXiv:1509.06581 [gr-qc].
- [44] R. Abbott *et al.* (KAGRA, VIRGO, LIGO Scientific), “Open Data from the Third Observing Run of LIGO, Virgo, KAGRA, and GEO,” *Astrophys. J. Suppl.* **267**, 29 (2023), arXiv:2302.03676 [gr-qc].
- [45] Connor McIsaac, Charlie Hoy, and Ian Harry, “Search technique to observe precessing compact binary mergers in the advanced detector era,” *Phys. Rev. D* **108**, 123016 (2023), arXiv:2303.17364 [gr-qc].
- [46] Alessandra Buonanno, Yan-bei Chen, and Michele Vallisneri, “Detecting gravitational waves from precessing binaries of spinning compact objects: Adiabatic limit,” *Phys. Rev. D* **67**, 104025 (2003), [Erratum: *Phys.Rev.D* 74, 029904 (2006)], arXiv:gr-qc/0211087.
- [47] Bruce Allen, Warren G. Anderson, Patrick R. Brady, Duncan A. Brown, and Jolien D. E. Creighton, “FINDCHIRP: An Algorithm for detection of gravitational waves from inspiraling compact binaries,” *Phys. Rev. D* **85**, 122006 (2012), arXiv:gr-qc/0509116.
- [48] S. Babak *et al.*, “Searching for gravitational waves from binary coalescence,” *Phys. Rev. D* **87**, 024033 (2013), arXiv:1208.3491 [gr-qc].
- [49] Stanislaw Babak, “Building a stochastic template bank for detecting massive black hole binaries,” *Class. Quant. Grav.* **25**, 195011 (2008), arXiv:0801.4070 [gr-qc].
- [50] Ian W. Harry, Bruce Allen, and B. S. Sathyaprakash, “A Stochastic template placement algorithm for gravitational wave data analysis,” *Phys. Rev. D* **80**, 104014 (2009), arXiv:0908.2090 [gr-qc].
- [51] Geraint Pratten, Sascha Husa, Cecilio Garcia-Quiros, Marta Colleoni, Antoni Ramos-Buades, Hector Estelles, and Rafel Jaume, “Setting the cornerstone for a family of models for gravitational waves from compact binaries: The dominant harmonic for nonprecessing quasicircular black holes,” *Phys. Rev. D* **102**, 064001 (2020), arXiv:2001.11412 [gr-qc].
- [52] Cecilio García-Quirós, Marta Colleoni, Sascha Husa, Héctor Estellés, Geraint Pratten, Antoni Ramos-Buades, Maite Mateu-Lucena, and Rafel Jaume, “Multimode frequency-domain model for the gravitational wave signal from nonprecessing black-hole binaries,” *Phys. Rev. D* **102**, 064002 (2020), arXiv:2001.10914 [gr-qc].
- [53] B. P. Abbott *et al.* (KAGRA, LIGO Scientific, Virgo), “Prospects for observing and localizing gravitational-wave transients with Advanced LIGO, Advanced Virgo and KAGRA,” *Living Rev. Rel.* **19**, 1 (2016), arXiv:1304.0670 [gr-qc].
- [54] Alex Nitz, Ian Harry, Duncan Brown, Christopher M. Biwer, Josh Willis, Tito Dal Canton, Collin Capano, Thomas Dent, Larne Pekowsky, Gareth S Cabourn Davies, Soumi De, Miriam Cabero, Shichao Wu, Andrew R. Williamson, Bernd Machenschalk, Duncan Macleod, Francesco Pannarale, Prayush Kumar, Steven Reyes, dfinstad, Sumit Kumar, Márton Tápai, Leo Singer, Praveen Kumar, veronica villa, maxtrevor, Bhooshan Uday Varsha Gadre, Sebastian Khan, Stephen Fairhurst, and Arthur Tolley, “gwastro/pycbc,” (2025).
- [55] Alexander Harvey Nitz, “Distinguishing short duration noise transients in LIGO data to improve the PyCBC search for gravitational waves from high mass binary black hole mergers,” *Class. Quant. Grav.* **35**, 035016 (2018), arXiv:1709.08974 [gr-qc].
- [56] S. Mozzon, L. K. Nuttall, A. Lundgren, T. Dent,

- S. Kumar, and A. H. Nitz, “Dynamic Normalization for Compact Binary Coalescence Searches in Non-Stationary Noise,” *Class. Quant. Grav.* **37**, 215014 (2020), arXiv:2002.09407 [astro-ph.IM].
- [57] Praveen Kumar and Thomas Dent, “Optimized search for a binary black hole merger population in LIGO-Virgo O3 data,” *Phys. Rev. D* **110**, 043036 (2024), arXiv:2403.10439 [gr-qc].
- [58] R. Abbott *et al.* (LIGO Scientific, VIRGO), “GWTC-2.1: Deep extended catalog of compact binary coalescences observed by LIGO and Virgo during the first half of the third observing run,” *Phys. Rev. D* **109**, 022001 (2024), arXiv:2108.01045 [gr-qc].
- [59] Vaibhav Tiwari, “Estimation of the Sensitive Volume for Gravitational-wave Source Populations Using Weighted Monte Carlo Integration,” *Class. Quant. Grav.* **35**, 145009 (2018), arXiv:1712.00482 [astro-ph.HE].
- [60] Rahul Dhurkunde, “Data Release: Search for Precessing Binary Black Holes in Advanced LIGO’s Third Observing Run using Harmonic Decomposition,” <https://github.com/rahuldhurkunde/O3-precessing-BBH-search> (2026).
- [61] Mark Hannam, Patricia Schmidt, Alejandro Bohé, Leïla Haegel, Sascha Husa, Frank Ohme, Geraint Pratten, and Michael Pürrer, “Simple Model of Complete Precessing Black-Hole-Binary Gravitational Waveforms,” *Phys. Rev. Lett.* **113**, 151101 (2014), arXiv:1308.3271 [gr-qc].
- [62] Hang Yu, Javier Roulet, Tejaswi Venumadhav, Barak Zackay, and Matias Zaldarriaga, “Accurate and efficient waveform model for precessing binary black holes,” *Phys. Rev. D* **108**, 064059 (2023), arXiv:2306.08774 [gr-qc].
- [63] Marta Colleoni, Felip A. Ramis Vidal, Cecilio García-Quirós, Sarp Akçay, and Sayantani Bera, “Fast frequency-domain gravitational waveforms for precessing binaries with a new twist,” *Phys. Rev. D* **111**, 104019 (2025), arXiv:2412.16721 [gr-qc].